JACS
JOURNAL OF THE AMERICAN CHEMICAL SOCIETY

Article

pubs.acs.org/JACS

Reversible CO Scavenging via Adsorbate-Dependent Spin State Transitions in an Iron(II)–Triazolate Metal–Organic Framework

Douglas A. Reed,[†] Dianne J. Xiao,[†] Miguel I. Gonzalez,[†] Lucy E. Darago,[†] Zoey R. Herm,[†] Fernande Grandjean,[‖] and Jeffrey R. Long*[,†,‡,§]

[†]Department of Chemistry, and [‡]Department of Chemical and Biomolecular Engineering, University of California, Berkeley, California 94720, United States

[§]Materials Sciences Division, Lawrence Berkeley National Laboratory, Berkeley, California 94720, United States

[‖]Department of Chemistry, Missouri University of Science and Technology, University of Missouri, Rolla, Missouri 65409, United States

Supporting Information

ABSTRACT: A new metal–organic framework, Fe-BTTri ($Fe_3[(Fe_4Cl)_3(BTTri)_8]_2 \cdot 18CH_3OH$, H_3BTTri =1,3,5-tris(1*H*-1,2,3-triazol-5-yl)benzene)), is found to be highly selective in the adsorption of CO over a variety of other gas molecules, making it extremely effective, for example, in the removal of trace CO from mixtures with H_2, N_2, and CH_4. This framework not only displays significant CO adsorption capacity at very low pressures (1.45 mmol/g at just 100 μbar), but, importantly, also exhibits readily reversible CO binding. Fe-BTTri utilizes a unique spin state change mechanism to bind CO in which the coordinatively unsaturated, high-spin Fe^{II} centers of the framework convert to octahedral, low-spin Fe^{II} centers upon CO coordination. Desorption of CO converts the Fe^{II} sites back to a high-spin ground state, enabling the facile regeneration and recyclability of the material. This spin state change is supported by characterization via infrared spectroscopy, single crystal X-ray analysis, Mössbauer spectroscopy, and magnetic susceptibility measurements. Importantly, the spin state change is selective for CO and is not observed in the presence of other gases, such as H_2, N_2, CO_2, CH_4, or other hydrocarbons, resulting in unprecedentedly high selectivities for CO adsorption for use in CO/H_2, CO/N_2, and CO/CH_4 separations and in preferential CO adsorption over typical strongly adsorbing gases like CO_2 and ethylene. While adsorbate-induced spin state transitions are well-known in molecular chemistry, particularly for CO, to our knowledge this is the first time such behavior has been observed in a porous material suitable for use in a gas separation process. Potentially, this effect can be extended to selective separations involving other π-acids.

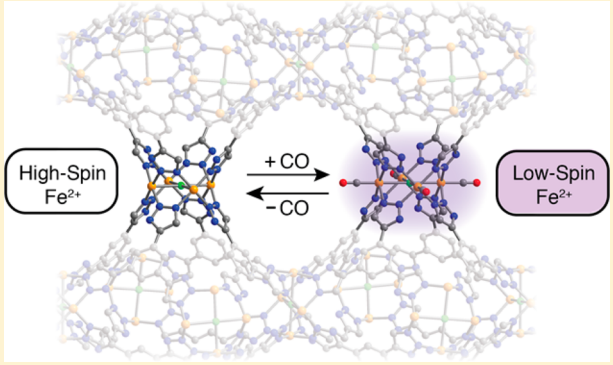

INTRODUCTION

Metal–organic frameworks are a class of permanently porous materials exhibiting tremendous chemical tunability and high internal surface areas.[1] An important subset of these materials features high densities of exposed metal cation sites (i.e., metal centers that preserve open coordination sites upon desolvation of the framework). These exposed metal sites typically act as Lewis acids that can accept electron density from easily polarized gas molecules such as CO_2. This electrostatic interaction is the underlying basis for a wide variety of potential applications in gas storage and separations.[2] However, many gas molecules can behave as π-acids in addition to σ-donors, and developing frameworks that take advantage of this additional property could lead to new adsorbents displaying unprecedented selectivities in separations involving carbon monoxide, unsaturated hydrocarbons, and other small molecules with low-lying π^* orbitals. In order to bind such species strongly, a material needs to possess exposed transition metal centers that function not just as exposed partial positive charges, but as sites capable of π back-donation.[3] Unfortunately, this feature has been difficult to realize in practice, since the majority of frameworks with open metal sites are ligated by weak-field carboxylate or aryl-oxide ligands, resulting in electron-poor, high-spin metal centers that are only weakly π-donating. As a result, only a small number of metal–organic frameworks feature exposed electron-rich, low-spin first-row transition metal centers suitable for π back-donation.[4]

An important application of porous materials containing π-donating exposed metal sites is in the area of carbon monoxide separations, and new adsorbent-based technologies can be envisioned for both CO removal as well as CO purification. For

Received: January 8, 2016
Published: April 20, 2016

DOI: 10.1021/jacs.6b00248
J. Am. Chem. Soc. 2016, 138, 5594–5602

example, trace CO removal from H_2 is relevant to both ammonia production and fuel cell technologies, as even ppm levels (often <10 ppm) of CO can poison the catalysts used in these applications.[5] Aside from CO scrubbing, CO is produced in large quantities from processes such as iron and steel production, coke production and coal gasification, partial oxidation processes, and steam reforming of methane, appearing in mixtures containing H_2, N_2, CO_2, and various hydrocarbons. Carbon monoxide is a valuable chemical precursor used in the production of several commodity chemicals, including alcohols, monomers and polymers, and acetic acid, and the efficient separation of pure CO from these gas mixtures would allow for the use of CO as a versatile carbon synthon.[6] Currently, CO separations are achieved via cryogenic distillation, although membrane,[7] adsorption,[8] and liquid adsorption[9] based processes have also been investigated. While some metal−organic frameworks or similar materials have been studied for CO adsorption,[10] most of these materials do not bind CO strongly enough to remove trace amounts or leverage the π-acidity of CO to selectively adsorb it over a variety of gas molecules. Other frameworks bind CO so strongly that adsorption is irreversible, limiting their use in practical applications.[11]

In order to achieve highly selective CO binding while retaining good reversibility, we envisioned a material in which the exposed metal center could interconvert between high-spin and low-spin configurations. A low-spin metal center would afford an elusive electron donating metal species capable of strong CO interactions for trace CO removal and selective CO adsorption over polarizable gas molecules that are typically adsorbed strongly by metal−organic frameworks, while the ability to convert back to high-spin would also allow for facile desorption of CO due to the much weaker metal−carbonyl interaction. To date, only a small number of metal−organic frameworks display the ability to undergo reversible spin transitions and retain their porosity,[12] and none feature accessible, coordinatively unsaturated metal sites. We hypothesized that a framework with exposed Fe^{II} centers in a triazolate-based coordination environment would be a promising material, due to the large number of spin-crossover Fe^{II}−triazole and Fe^{II}−triazolate complexes.[13] Specifically, an iron analogue of a triazolate-based copper framework previously synthesized in our laboratory, $H[(Cu_4Cl)_3(BTTri)_8]$ (Cu-BTTri, H_3BTTri = 1,3,5-tris(1*H*-1,2,3-triazol-5-yl)benzene)), was targeted due to its high concentration of open metal sites coordinated by triazolates.[14] Herein, we report the new metal−organic framework, $Fe_3[(Fe_4Cl)_3(BTTri)_8]_2\cdot 18CH_3OH$ (Fe-BTTri), featuring coordinatively unsaturated Fe^{II} centers that can indeed reversibly convert from a high-spin to a low-spin electron configuration upon exposure to carbon monoxide. As a result, the material shows unprecedented selectivity for the adsorption of CO over H_2, especially at low concentrations of CO, while also displaying preferential adsorption of CO over N_2, CO_2, ethylene, and a variety of other molecules.

MATERIALS AND METHODS

General Information. All manipulations were performed under an N_2 atmosphere in a VAC Atmospheres glovebox or using standard Schlenk techniques. The compound H_3BTTri was prepared according to a previously reported procedure.[14] $FeCl_2$ was purchased from Sigma-Aldrich and used as received. Dimethylformamidium trifluoromethanesulfonate was purchased from Sigma-Aldrich and dried under vacuum prior to use. Methanol was purchased from EMD Millipore Corporation as DriSolv grade, dried over 3 Å sieves, and sparged with Ar prior to use. Dimethylformamide (DMF) was purchased from EMD Millipore Corporation as OmniSolv grade, sparged with Ar, and dried with an alumina column prior to use.

$Fe_3[(Fe_4Cl)_3(BTTri)_8]_2\cdot 18CH_3OH$ (Fe-BTTri). To a 25 mL Schlenk flask charged with a stir bar and a solution of H_3BTTri (50 mg, 1.0 equiv, 0.18 mmol) and dimethylformamidium trifluoromethanesulfonate (180 mg, 4.5 equiv, 0.81 mmol) in DMF (8 mL) was added a solution of $FeCl_2$ (230 mg, 10 equiv, 1.8 mmol) in 2 mL of methanol. The yellow solution was stirred at 120 °C for 10 days. The resulting yellow powder was collected by filtration, rinsed with DMF, and soaked in 10 mL of DMF at 120 °C for 12 h. The supernatant solution was decanted, and 10 mL of fresh DMF was added. This process was repeated nine times so that the total time washing with DMF was 5 days. The yellow powder was collected by filtration, rinsed with methanol, and soaked in 10 mL of methanol at 60 °C for 12 h. The supernatant solution was decanted, and 10 mL of fresh methanol was added. This process was repeated nine times so that the total time washing with methanol was 5 days. The resulting yellow powder was collected by filtration, and heated at 180 °C under dynamic vacuum (<0.01 mbar) for 2 days, affording 50 mg (66%) of product as a tan powder. Elemental analysis of bulk sample ($C_{210}H_{168}Cl_6Fe_{27}N_{144}O_{18}$): Found: C, 37.40; H, 2.20; N, 30.05. Calculated: C, 37.53; H, 2.52; N, 30.03.

Single Crystals of Fe-BTTri. To a stainless steel bomb charged with a solution of H_3BTTri (12 mg, 2.2 equiv, 0.043 mmol) and dimethylformamidium trifluoromethanesulfonate (24 mg, 5.4 equiv, 0.11 mmol) in DMF (8 mL) was added a solution of $FeCl_2$ (2.5 mg, 1.0 equiv, 0.020 mmol) in methanol (2 mL). The solution was heated at 160 °C for 3 days. Small yellow crystals were isolated by decanting the supernatant solution, rinsed with DMF, and soaked in 10 mL of DMF at 120 °C for 12 h. The supernatant solution was decanted, and 10 mL of fresh DMF was added. This process was repeated four times so that the total time washing with DMF was 5 days. The yellow crystals were collected by filtration, rinsed with methanol, and soaked in 10 mL of methanol at 60 °C for 12 h. The supernatant solution was decanted, and 10 mL of fresh methanol was added. This process was repeated nine times, so that the total time washing with methanol was 5 days. The yellow crystals were collected by filtration, and heated at 150 °C under dynamic vacuum (<0.01 mbar) for 2 days, affording ∼2 mg of pale red crystals of Fe-BTTri.

RESULTS AND DISCUSSION

Synthesis of Fe-BTTri. A solvated form of the new metal−organic framework $Fe_3[(Fe_4Cl)_3(BTTri)_8]_2\cdot 18CH_3OH$ (Fe-BTTri) was isolated as a yellow, microcrystalline powder from the reaction between $FeCl_2$ and H_3BTTri in DMF and methanol. The compound can be mostly desolvated by first soaking in methanol to remove DMF, followed by heating at 180 °C under dynamic vacuum to yield activated Fe-BTTri as a tan powder. The powder is microcrystalline and retains its crystallinity through activation, as assessed by powder X-ray diffraction measurements (Figure S1). The resulting X-ray diffraction pattern indicates a framework structure type analogous to that of Cu-BTTri.[14] The activated material retains a small amount of methanol, as seen by elemental analysis, and the majority of these methanol molecules are postulated to be bound to the extra-framework Fe^{II} cations. Adsorption of N_2 at 77 K revealed a Langmuir surface area of 1930 m^2/g and a Brunauer−Emmett−Teller (BET) surface area of 1630 m^2/g (Figure S3). These values are in good agreement with results obtained for Cu-BTTri, which displays Langmuir and BET surface areas of 1900 and 1770 m^2/g, respectively.[14]

Cubic single crystals suitable for X-ray diffraction can be grown under similar conditions using more dilute iron and ligand concentrations and more acidic conditions. The DMF solvated form of a Fe-BTTri crystal displays $Fm\bar{3}c$ symmetry,

DOI: 10.1021/jacs.6b00248
J. Am. Chem. Soc. 2016, 138, 5594−5602

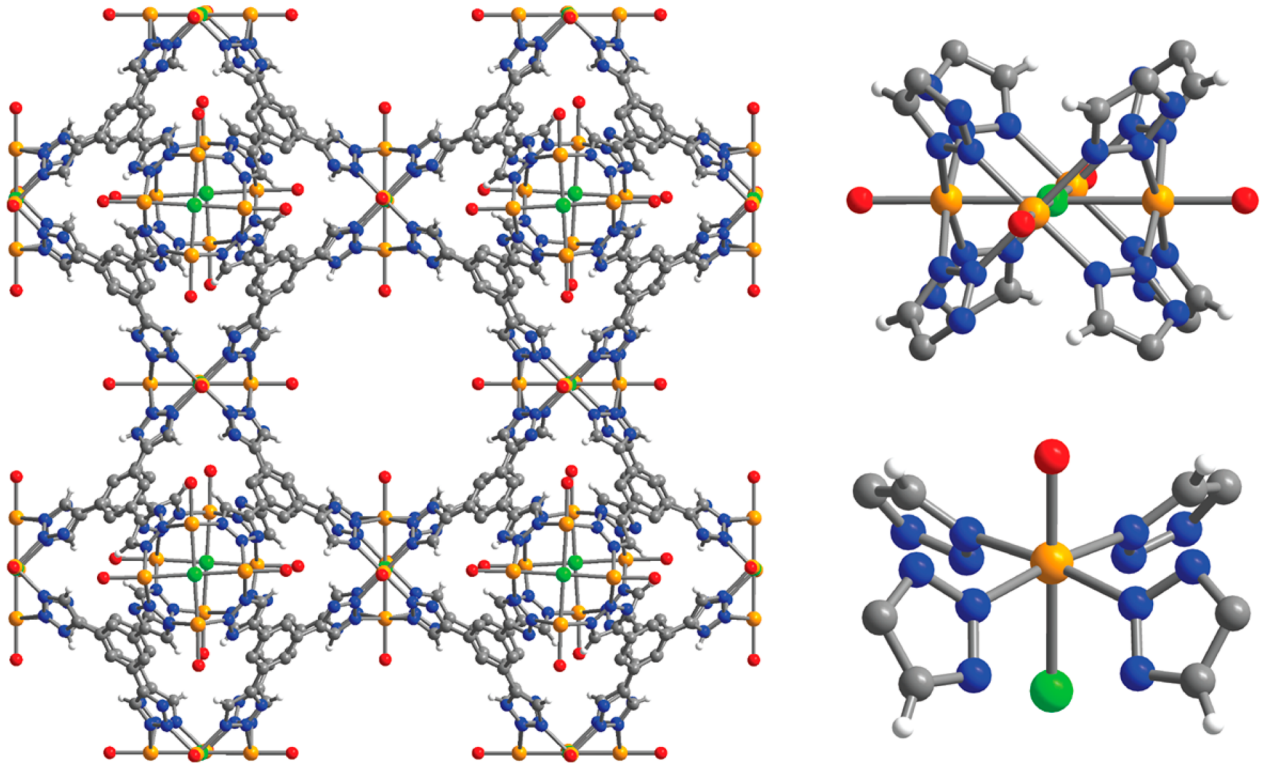

Figure 1. Portion of the structure of DMF-solvated Fe-BTTri (left) as determined by analysis of single-crystal X-ray diffraction data. Structures of $[Fe_4Cl]^{7+}$ (upper right) and a single iron site (lower right) of DMF-solvated Fe-BTTri. Orange, gray, blue, red, green, and white spheres represent Fe, C, N, O, Cl, and H atoms, respectively; some H atoms and C and N atoms on iron-bound DMF molecules are omitted for clarity.

composed of six square, chloride-centered $[Fe_4Cl]^{7+}$ units and eight trigonal $BTTri^{3-}$ ligands that combine to form truncated octahedra, creating a sodalite-like cage (Figure 1). Numerous frameworks of this type, commonly referred to as M-BTT (M = Mn, Fe, Co, Ni, Cu, Cd), have been realized using the analogous tetrazolate ligand 1,3,5-benzenetristetrazolate (BTT^{3-}).[15] Interestingly, the less symmetric triazolate groups are well ordered within Fe-BTTri, with the H atoms of each triazolate unit oriented in the same direction around a crystallographic 4-fold rotation axis on which the $[Fe_4Cl]^{7+}$ unit resides. This ordering is likely a result of the framework connectivity disfavoring steric repulsion between H atoms on adjacent triazolates. The resulting arrangement creates a slight twist of the triazoles around the $[Fe_4Cl]^{7+}$ unit, which is not observed in M-BTT structures, and causes opposite squares on each truncated octahedron to be offset by approximately 6°. The location of the charge balancing extra-framework Fe^{II} cations within the pores of the framework could not be determined from the electron difference map obtained from the X-ray diffraction data. Structural characterization of the activated material could not be achieved under standard single crystal experimental conditions, as ambient solvent rapidly binds to the open iron sites prior to data collection. However, the single crystals retain their crystallinity upon heating to 150 °C, indicating that the material is thermally stable.

Gas Adsorption. The compound Fe-BTTri was investigated for selected gas adsorption properties. In particular, adsorption isotherms for CO were collected at various temperatures. As shown in Figure 2, the CO adsorption isotherm at 25 °C shows an extremely steep initial rise, reaching a value of 1.49 mmol/g adsorbed at just 102 μbar. The sharp initial uptake ends at 2.2 mmol/g at 157 μbar, and subsequent uptake more gradually increases to 2.7 mmol/g at 268 mbar, corresponding to a maximum total adsorption of CO at 75% of the iron sites (excluding extra-framework Fe^{II} cations). The steep rise in the isotherm suggests an initial strong interaction with CO for some of the iron sites, whereas the gradual rise afterward represents weak interactions with the framework. The remaining iron sites are likely blocked by solvent or remain inaccessible, as has been observed previously for Fe-BTT.[15c] This sharp uptake of CO adsorption is also seen at higher temperatures, with significant adsorption of CO still observable at 100 °C, reaching 1.08 mmol/g at 1.06 mbar.

The adsorption of CO at different temperatures was examined to evaluate the strength of its binding within the framework. Isotherms collected from 25 to 150 °C all displayed significant low-pressure adsorption relative to other CO adsorbing materials (Figure 2). By fitting isotherms collected from 65 to 100 °C with a Langmuir−Freundlich equation and employing the Clausius−Clapeyron relation, an isosteric heat of adsorption (Q_{st}) of −65 kJ/mol can be calculated (Figure S7). This value is greater in magnitude than those previously reported for metal−organic frameworks examined for CO adsorption, which have isosteric heats of adsorption ranging from −19 to −52 kJ/mol.[10] The isosteric heat of adsorption, combined with a high capacity for CO at low pressures, suggests that Fe-BTTri is a promising candidate for extracting and removing very low concentrations of CO from gas mixtures. Indeed, its CO adsorption capacity of 0.75 mmol/g at just 0.05 mbar is unprecedented for these materials, representing a 2 orders of magnitude improvement relative to the previous best material, Ni_2(dobdc) ($dobdc^{4-}$ = 2,5-dioxido-1,4-benzene-dicarboxylate) (Figure S8).[10d] It should be noted, however, that the adsorption capacity of Fe-BTTri at pressures

DOI: 10.1021/jacs.6b00248
J. Am. Chem. Soc. 2016, 138, 5594−5602

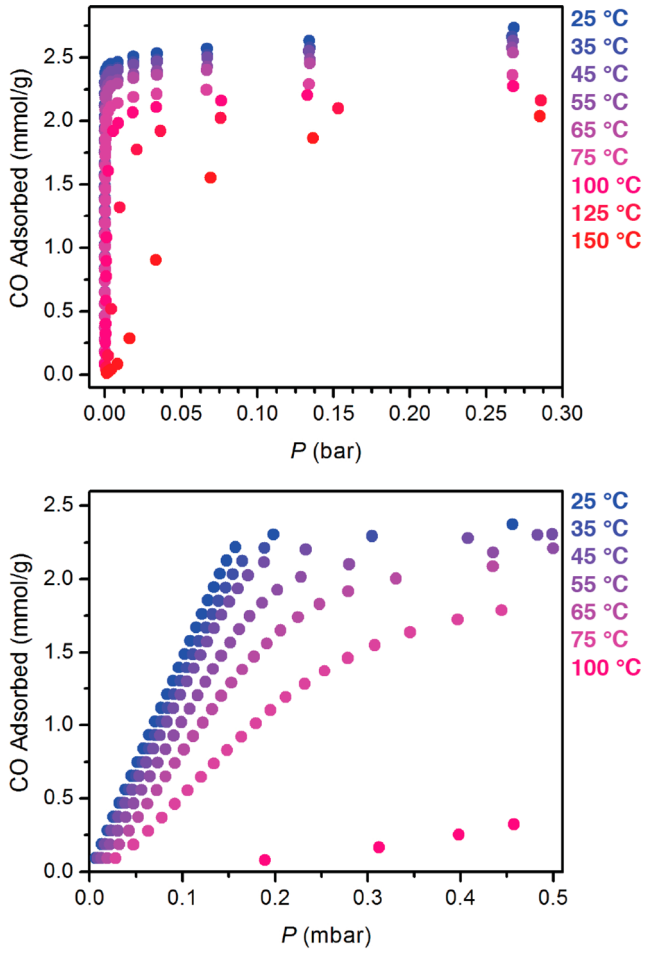

Figure 2. Excess carbon monoxide isotherms measured at various temperatures in Fe-BTTri (upper). Detail of low-pressure region (lower).

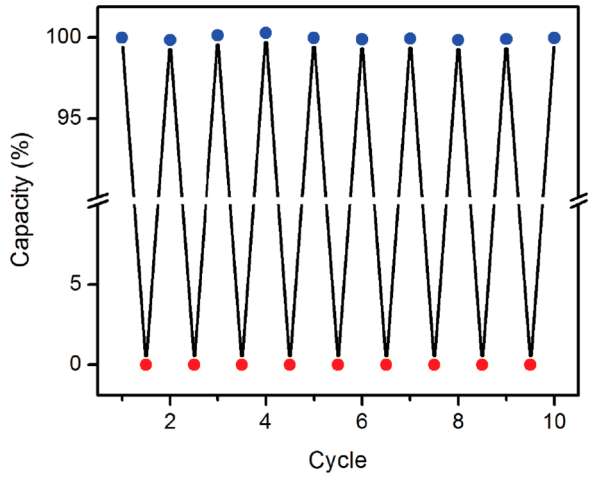

Figure 3. Cycling data of successive adsorption and desorption of carbon monoxide in Fe-BTTri, with adsorption expressed in terms of percentage of the capacity observed for cycle 1. Adsorption (blue circles) occurred within 10 min upon dosing CO at 25 °C at 10 mbar, and complete desorption (red circles) was accomplished by heating the sample at 150 °C under dynamic vacuum for 5 min.

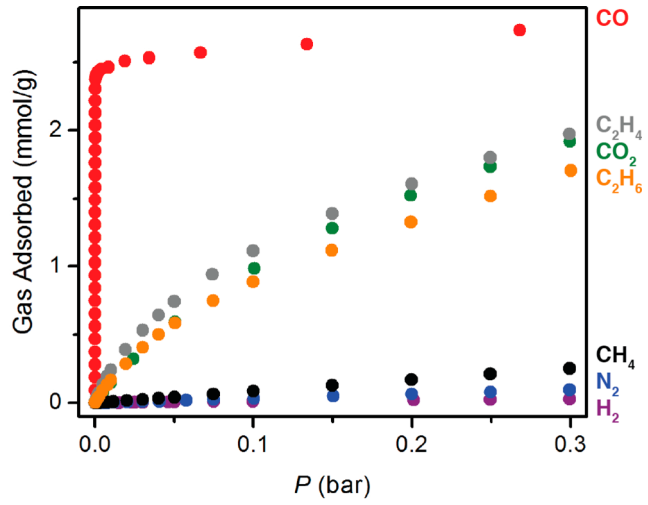

Figure 4. Excess gas adsorption isotherms collected at 25 °C for Fe-BTTri.

greater than 268 mbar is lower than that of Ni_2(dobdc) and several related materials because of its lower concentration of accessible open metal sites.[10d]

Remarkably, despite the strong binding of CO, ready desorption of the adsorbed CO can be accomplished by heating CO-dosed Fe-BTTri under dynamic vacuum at 150 °C for as little as 5 min. No loss in CO capacity is observed even after 10 cycles (Figure 3). At lower temperatures, full reactivation can be achieved by using slightly longer activation times (e.g., 30 min at 100 °C) (Figure S9). Thus, Fe-BTTri offers the possibility of serving as a readily regenerable scavenger for removing CO from gas mixtures.

To assess the ability of Fe-BTTri to separate CO from mixed CO/H_2 gas streams for the purification of hydrogen, H_2 adsorption isotherms were also collected. At 25 °C, only a very minor uptake of H_2 is observed, with the isotherm rising gradually to reach a value of 0.05 mmol/g at 1.0 bar (Figure 4). Indeed, at all of the pressures evaluated, Fe-BTTri was found to adsorb significantly more CO than H_2, suggesting its application in the selective adsorption of CO during hydrogen purification.

In order to evaluate the separation capabilities, Ideal Adsorbed Solution Theory (IAST) was used to calculate selectivity factors for a hypothetical mixed gas stream containing a variety of different gas compositions at a total pressure of 1 bar at 25 °C. For all calculated CO/H_2 mixtures, Fe-BTTri shows very high IAST selectivity values. At low concentrations of CO in a mixture with H_2 (5% CO at a total pressure of 1 bar), IAST predicts a selectivity of 7400 for CO over H_2, over 40% higher than the value calculated for Ni_2(dobdc), and among the best values for any mixed gas separation with a metal−organic framework (Figure 5).[10d] CO concentrations in H_2 streams can be as low as 1−3%, and at these concentrations for 1 bar total pressure, IAST predicts even higher selectivities of 10 900 at 3% CO and 24 800 at 1% CO. Importantly, the strong upward trend toward lower concentrations of CO suggests Fe-BTTri is a very promising CO scrubbing material. For fuel cell technologies and other applications sensitive to even ppm levels of CO, one can envision performing these separations at higher pressures or different temperatures to achieve nearly complete CO removal. It should be noted that these values are particularly sensitive to the accuracy of the H_2 isotherm fit, and fitting the isotherm with different saturation capacities changes these selectivity values slightly (Figure S11). However, these IAST values

DOI: 10.1021/jacs.6b00248
J. Am. Chem. Soc. 2016, 138, 5594−5602

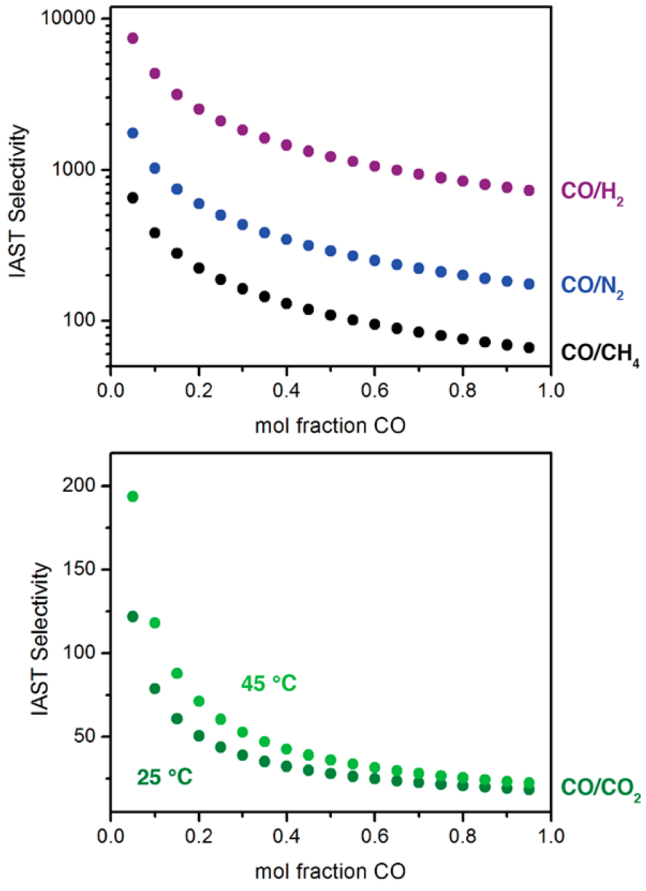

Figure 5. Ideal adsorbed solution theory (IAST) selectivities for mixtures of CO/H_2 (purple), CO/N_2 (blue) and CO/CH_4 (black) at varying concentrations at 25 °C and 1 bar of total pressure in Fe-BTTri (upper). IAST selectivites for mixtures of CO/CO_2 at varying concentrations and 1 bar total pressure at 25 °C (dark green) and 45 °C (light green) (lower).

remain significantly higher than all previously reported CO adsorbing materials for several different isotherm fits for H_2.

The purity of the adsorbed phase in these separations was also examined, as the adsorbed CO can also be used as a feedstock in a variety of industrial processes. The IAST values for CO/H_2 mixtures suggest that Fe-BTTri could be used to obtain very pure CO, with purities ranging from 99.6% at the very lowest concentration of CO (1% CO in a CO/H_2 mixture at 1 bar total pressure), to 99.99% at higher CO concentrations. In examining the ability of Fe-BTTri to separate CO from other gas streams, such as mixtures with N_2, CO_2, CH_4, C_2H_6, and C_2H_4, additional adsorption isotherms were measured (Figure 4). For CH_4 and N_2 at 25 °C, the isotherms rise gradually to 0.69 and 0.26 mmol/g at 1.0 bar, respectively. For all pressures measured Fe-BTTri adsorbs significantly more CO, leading to high calculated IAST selectivities. For mixtures with N_2, these values are as high as 1750 for a 1 bar mixture containing 0.05 mole fraction of CO (Figure 5), corresponding to 98.9% pure CO in the adsorbed phase at room temperature. Importantly, this is much more practical than the very low temperature (120 K) required for other frameworks that exhibit this selectivity.[10c] Notably, this IAST value is also over 200% higher than that calculated for Ni_2(dobdc), which also exhibits the ability to separate CO and N_2 at room temperature.[10d] Selectivities are similarly high for mixtures with CH_4, with IAST values approaching as high as 650 for a 0.05 mole fraction of CO in a 1 bar total CO/CH_4 mixture, corresponding to 97.1% adsorbed CO. Both CO/N_2 and CO/CH_4 selectivities in Fe-BTTri approach 99.9% CO on the adsorbed phase at higher concentrations of CO in hypothetical CO/N_2 and CO/CH_4 mixtures, indicating the significant promise of this material for collecting pure CO from gas streams.

For CO_2, C_2H_6, and C_2H_4, the 25 °C isotherms rise gradually to 3.52, 3.83, and 3.64 mmol/g at 1.0 bar, respectively (Figure 4). While the uptake is significant, the low-pressure (<300 mbar) uptake is much more gradual than that observed for CO adsorption, suggesting that useful selectivities can be achieved. Indeed, for Fe-BTTri, an IAST selectivity of 121 is calculated for a 0.05 mole fraction of CO in a 1 bar mixture with CO_2 at 25 °C (Figure 5). In addition, because of the strong binding of CO relative to CO_2, raising the temperature from 25 to 45 °C increases the IAST selectivity significantly, going from 121 to 193 for a 5:95 $CO:CO_2$ mixture at 1 bar total pressure. This temperature dependence of the IAST selectivity is also observed in CO/C_2H_4 and CO/C_2H_6 mixtures, with calculated selectivity values similar to those observed for CO/CO_2 separations (Figures S13 and S15). Importantly, these values still translate to very pure CO in the adsorbed phase, as 50% CO in mixtures of CO/C_2H_6, CO/CO_2, and CO/C_2H_4 at 25 °C at 1 bar total pressure are expected to result in 93.2–96.5% CO in the adsorbed phase, respectively, and increase upon raising the temperature, reaching 95.9–98.1% at 45 °C under the same conditions. Indeed, Fe-BTTri shows the ability to separate CO from a variety of different gas mixtures, even in mixtures with ethylene and CO_2 that are very competitive in other metal–organic frameworks, and retains high purity CO in the adsorbed phase.

Infrared Spectroscopy. To understand the origin of the strong CO selectivity observed in Fe-BTTri, various spectroscopic methods were employed to probe the state of both the framework iron sites and the bound CO molecules. Infrared spectroscopy was used as an initial probe for the nature of the iron–carbonyl interaction. After exposure to 0.05 bar of CO, a sharp absorbance band at 2017 cm^{-1} arises (Figure 6). This C–O stretching frequency is red-shifted relative to free CO (2143 cm^{-1}), indicating π back-donation into the π^* orbital of the carbonyl.

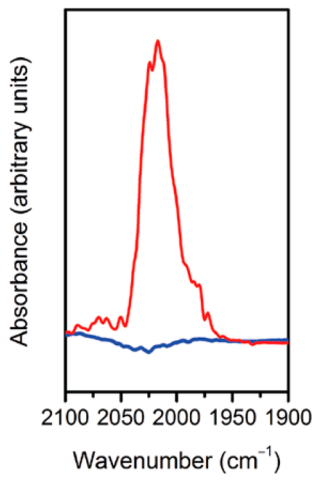

Figure 6. Infrared spectra collected at 25 °C for Fe-BTTri (blue) and CO-dosed Fe-BTTri (red).

DOI: 10.1021/jacs.6b00248
J. Am. Chem. Soc. 2016, 138, 5594–5602

To date, a red-shift in the carbonyl stretching frequency has only been observed for metal−organic frameworks that irreversibly bind CO.[11] Indeed, all metal−organic frameworks that have been characterized so far for reversible CO adsorption display blue-shifted stretching frequencies, with values ranging from 2160 to 2190 cm^{-1}, indicating a weak interaction with a high-spin metal center acting predominantly as a Lewis acid.[10b−d,16] In distinct contrast, the value observed for CO-dosed Fe-BTTri is more consistent with several known low-spin molecular Fe^{II} species in similar ligand environments, such as those observed in various CO-bound Fe^{II} porphyrins or other nitrogen-containing square-planar tetradentate ligands.[17] This indicates that upon binding CO the Fe^{II} sites of Fe-BTTri are low-spin, which to date has not been seen in a metal−organic framework with reversible CO adsorption.

Spin State Characterization. Since the CO stretching frequency suggested a conversion from high-spin to low-spin Fe^{II} upon adsorption of CO, Mössbauer spectroscopy and dc magnetic susceptibility were utilized to probe directly the metal spin states in the activated Fe-BTTri and the CO-dosed framework. For the activated material, the Mössbauer spectrum at 100 K (Figure 7) reveals several high-spin Fe^{II} species, with isomer shifts, δ, between 1.05 and 1.07 mm/s and quadrupole splitting values, ΔE_Q, between 1.80 and 3.06 mm/s. The existence of several slightly different iron sites is attributed to the distribution of residual solvent and extra-framework cations throughout the framework, which, as observed previously in related frameworks, can subtlely alter the environment of the Fe^{II} sites.[15c] While solvation with DMF did not increase the resolution for determination of distinct iron sites (Figure S17), both the activated and DMF-solvated Fe-BTTri profiles are readily fit using standard high-spin parameters, thus confirming the high-spin ground state for the Fe^{II} centers within the activated framework.[13c,d,15c,18] Upon increasing the temperature from 100 to 290 K, the isomer shifts and quadrupole splittings decrease as expected for high-spin Fe^{II} (Figure S18).

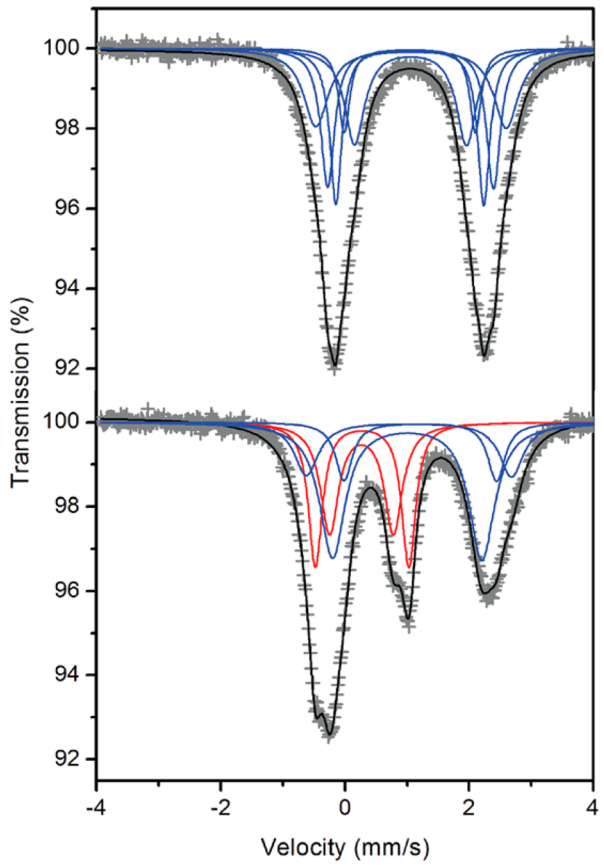

Figure 7. Mössbauer spectra collected at 100 K for Fe-BTTri (upper) and CO-dosed Fe-BTTri (lower), with the experimental data in gray plusses and the total fit in black. In both spectra, the blue components are assigned to high-spin Fe^{II}. In CO-dosed Fe-BTTri, the red components are assigned to low-spin Fe^{II}. The parameters for all components are listed in Table S6.

Activated Fe-BTTri was then dosed ex situ with 0.1 mbar of CO, and the 100 K Mössbauer spectrum exhibits a significantly different profile (Figure 7). Again, multiple different Fe^{II} components are required to reproduce the observed profile, however both high-spin and low-spin Fe^{II} species are observed. Here, high-spin Fe^{II} components, shown in blue, represent 58(3)% of the total absorption area and exhibit high-spin Fe^{II} with δ between 1.00 and 1.21 mm/s and ΔE_Q between 2.42 and 3.31 mm/s. These components are assigned to five-coordinate framework Fe^{II} sites and the extra-framework cations, which are not involved in CO binding. In contrast, a new set of doublets shown in red, representing 42(4)% of the total absorption area, exhibit significantly different hyperfine parameters, with both smaller δ of 0.26 and 0.27 mm/s and ΔE_Q between 1.03 and 1.50 mm/s. These hyperfine parameters are consistent with low-spin Fe^{II},[13c,d,18] strongly suggesting that upon binding CO the electron configuration of the Fe^{II} ions change from high-spin to low-spin. Remarkably, the total conversion to low-spin closely matches the uptake observed in the CO isotherm data at 0.1 mbar. Upon increasing the temperature from 100 to 290 K, the usual decrease in isomer shifts and quadrupole splittings is observed, but the percent area of the low-spin CO-bound Fe^{II} of 46(4)% remains constant within the accuracy of the measurements (Figure S19).

Magnetic measurements were also used to probe the spin state of the iron ions in Fe-BTTri. Dc magnetic susceptibility measurements performed under an applied magnetic field of 1 T were conducted for activated Fe-BTTri as well as samples dosed with various amounts of CO (Figure 8). For activated Fe-BTTri, the 300 K $\chi_M T$ value is expected to be 81 emu·K/mol for all high−spin Fe^{II} centers with $S = 2$ and $g = 2.00$. The observed $\chi_M T$ value at 300 K is 82.9 emu·K/mol, in good agreement with the calculated spin-only value. In order to confirm the high-spin nature of these iron sites in the bare framework, the data between 2 and 300 K was fit using the Hamiltonian shown in equation 1,

$$\hat{H} = -2J(\hat{S}_1\cdot\hat{S}_2 + \hat{S}_2\cdot\hat{S}_3 + \hat{S}_3\cdot\hat{S}_4 + \hat{S}_1\cdot\hat{S}_4) - 2J'(\hat{S}_1\cdot\hat{S}_3 + \hat{S}_2\cdot\hat{S}_4) + \sum_{i=1}^{4}\{D_i S_{iz}^2 + E_i(S_{ix}^2 + S_{iy}^2) + \mu_B g_i \hat{S}_i\cdot\hat{B}\} \quad (1)$$

which includes two isotropic coupling parameters and zero-field splitting and Zeeman terms. Magnetic coupling between nearest-neighbor Fe^{II} ions is represented by J, while the coupling between Fe^{II} sites located 180° from one another (i.e., coupling across the μ_4-Cl) is represented by J'. The Hamiltonian provided a good fit to the magnetic data in the temperature range 2−300 K using the parameters $|D_i| = 27$ cm^{-1}, $|E_i| = 0.01$ cm^{-1}, and $g_i = 2.40$, all for $i = 1-4$, and coupling constants of $J = -5.8$ cm^{-1} and $J' = -5.8$ cm^{-1}. High-

DOI: 10.1021/jacs.6b00248
J. Am. Chem. Soc. 2016, 138, 5594−5602

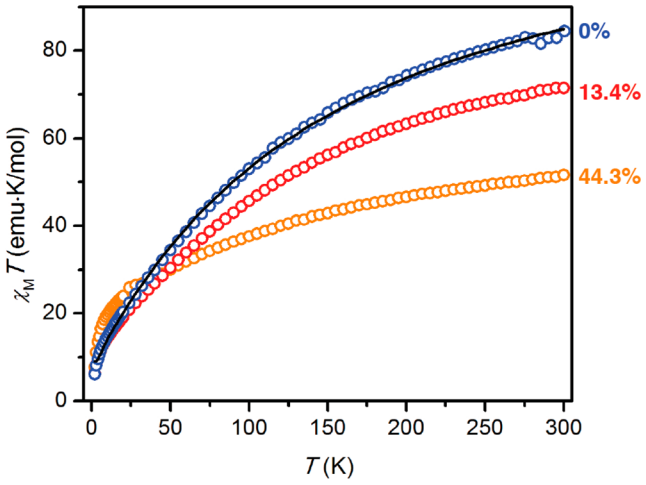

Figure 8. Variable-temperature magnetic susceptibility times temperature data collected under H_{dc} = 1 T for Fe-BTTri (blue), Fe-BTTri-$(CO)_{3.2}$ (13.4% CO-loaded, red), and Fe-BTTri-$(CO)_{10.6}$ (44.3% CO-loaded, orange). The black line represents a fit to the data employing a Hamiltonian and the parameters described in the text.

spin square pyramidal Fe^{II} systems have been predicted to exhibit significant magnetic anisotropy,[19] and similar $|D|$ values and g values greater than 2 have been observed for a number of high-spin square planar Fe^{II} complexes.[20] Although the coupling constants J and J' are expected to be different, coincidentally these values were found to be equivalent in the best fit of the data. This behavior has been seen in a similar molecular, pyrazolate bridged $Co^{II}_4(\mu_4\text{-Cl})$ square.[21] The magnetic analysis confirms that the Fe^{II} sites in Fe-BTTri can reasonably be classified as high-spin Fe^{II}.

Samples of Fe-BTTri loaded ex situ with CO were also investigated using magnetic susceptibility measurements. Materials with precisely dosed loadings of 13.4% and 44.3% of carbon monoxide per framework iron site were prepared using a gas adsorption analyzer. These materials, Fe-BTTri-$(CO)_{3.2}$ and Fe-BTTri-$(CO)_{10.6}$, respectively, exhibit decreased $\chi_M T$ values at 300 K compared to activated Fe-BTTri. The predicted $\chi_M T$ values for these loadings, assuming a spin state transition from S = 2 (high-spin) to S = 0 (low-spin) upon binding of CO to Fe^{II}, are 71.4 and 50.8 emu·K/mol for 13.4% and 44.3% CO loading, respectively. The observed values of 71.5 and 51.6 emu·K/mol are in good agreement with these predictions. Overall, both Mössbauer spectral and dc magnetic susceptibility measurements completely agree with the conversion of high-spin Fe^{II} to low-spin Fe^{II} upon CO binding.

Structural Characterization. Single-crystal X-ray diffraction data were collected for the DMF-solvated and CO-dosed forms of the Fe-BTTri. Owing to the conditions needed to collect and mount the crystals, a structure of the activated material could not be obtained, as ambient solvent was taken up at the vacant metal site prior to data collection. However, due to the high-spin nature of both the bare and DMF-solvated material, the structure of the activated material is likely similar to that of the DMF-solvated material, and comparisons to the CO-dosed structure can be made.

Ligated by DMF, the bond lengths associated with the metal centers are consistent with a high-spin Fe^{II} species. The Fe–O_{DMF} and the average Fe–N distances are 2.116(2) and 2.1424(14) Å, respectively, indicative of high-spin Fe^{II}.[22] These values are expected to be similar for activated Fe-BTTri, and are consistent with other high-spin Fe^{II} centers in metal–organic frameworks.[12a–i,15c]

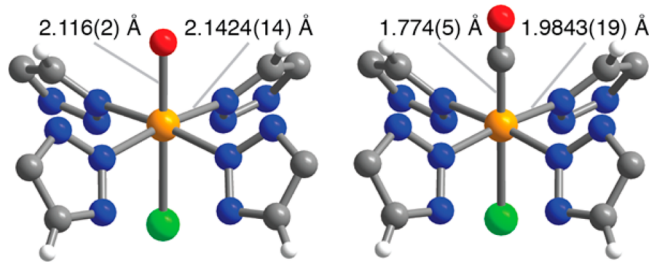

Figure 9. Portion of the structure of DMF-solvated Fe-BTTri (left) and CO-dosed Fe-BTTri-$(CO)_{24}$ (right), as determined by analysis of single-crystal X-ray diffraction data, with selected bond lengths highlighted. Numbers in parentheses give the estimated standard deviation in the final digits of the number. Orange, gray, red, blue, green, and white spheres represent Fe, C, O, N, Cl, and H atoms, respectively.

Upon ex situ dosing with CO, a significant structural change was observed (Figure 9). In Fe-BTTri-$(CO)_{24}$, the distances between the iron centers and the triazolate ligands contract to an average Fe–N distance of 1.9843(19) Å, a value that is consistent with low-spin Fe^{II}.[12a–i,13] In addition, the observed Fe–C_{CO} distance of 1.774(5) Å is very similar to reported literature values of octahedral low-spin Fe^{II}–CO complexes, such as the porphyrin complex Fe(TPP)CO(Py) (TPP = 5,10,15,20-tetraphenylporphyrin dianion, Py = pyridine), which exhibits a bond length of 1.77(2) Å, as well as other low-spin Fe^{II}–CO species.[22] Finally, the Fe–C–O linkage is essentially linear with an angle of 179.7(4)°, indicating a large degree of π orbital overlap. This is in contrast to structurally characterized high-spin (S = 2) Fe^{II}–CO adducts, which display nonlinear Fe–C–O linkages.[10d] These structural data, together with the infrared, Mössbauer, and magnetic results, confirm beyond any doubt that, upon binding CO, the Fe^{II} centers undergo a conversion from high- to low-spin, which to our knowledge has not previously been observed within a porous material.

CONCLUSIONS

The foregoing results demonstrate that Fe-BTTri engages in an unprecedented spin state change mechanism for the highly selective yet reversible binding of CO over H_2, N_2, CO_2, and various hydrocarbons. Indeed, IAST selectivity factors for these separations are among the highest values reported for any adsorbent-based gas separation, indicating the promise of this material for scavenging CO from various industrially relevant gas mixtures. Importantly, by leveraging the π-acidity of CO, Fe-BTTri is able to show preferential binding of CO over CO_2, ethylene, and other highly polarizable gas molecules that typically interact with Lewis-acidic open metal sites, as present in current metal–organic frameworks. The possibility of extending this spin-change mechanism to related frameworks and other gas molecules that might also have a strong interaction with low-spin Fe^{II}, such as olefins in olefin/paraffin separations, O_2 in O_2/N_2 separations, and N_2 in N_2/CH_4 separations, is now being investigated. Finally, since exposure to just trace amounts of CO induces changes in the structural, electronic, and spectral properties of Fe-BTTri, chemical identification and sensing are also promising avenues of exploration for this new type of material.

DOI: 10.1021/jacs.6b00248
J. Am. Chem. Soc. 2016, 138, 5594–5602

■ ASSOCIATED CONTENT

Supporting Information

The Supporting Information is available free of charge on the ACS Publications website at DOI: 10.1021/jacs.6b00248.

Crystallographic data for CO-dosed Fe-BTTri (CIF)
Crystallographic data for DMF-solvated Fe-BTTri (CIF)
Additional experimental details, adsorption data and analysis, powder X-ray diffraction data, single crystal X-ray diffraction data, crystal structure information, Mössbauer data, and magnetic susceptibility data (PDF)

■ AUTHOR INFORMATION

Corresponding Author

*jrlong@berkeley.edu

Notes

The authors declare no competing financial interest.

■ ACKNOWLEDGMENTS

This research was supported through the Center for Gas Separations Relevant to Clean Energy Technologies, an Energy Frontier Research Center funded by the U.S. Department of Energy, Office of Science, Office of Basic Energy Sciences under Award DE-SC0001015. Single-crystal X-ray diffraction experiments were performed at Beamline 11.3.1 at the Advanced Light Source, a DoE Office of Science User Facility operated by Lawrence Berkeley National Laboratory under Contract No. DE-AC02-05CH11231. Powder X-ray diffraction data were collected at Beamline 17-BM at the Advanced Photon Source, a DoE Office of Science User Facility, operated by Argonne National Laboratory under Contract DE-AC02-06CH11357. We thank Dr. B. K. Keitz, Dr. J. A. Mason, Dr. E. D. Bloch, and P. C. Bunting for helpful discussions, and we thank the NSF for providing graduate fellowship support for D.A.R., D.J.X., and L.E.D.

■ REFERENCES

(1) (a) Yaghi, O. M.; Li, H.; Eddaoudi, M.; O'Keefe, M. *Nature* **1999**, *402*, 276−279. (b) Kitagawa, S.; Kitaura, R.; Noro, S.-I. *Angew. Chem., Int. Ed.* **2004**, *43*, 2334−2375. (c) Matsuda, R.; Kitaura, R.; Kitagawa, S.; Kubota, Y.; Belosludov, R. V.; Kobayashi, T. C.; Sakamoto, H.; Chiba, T.; Takata, M.; Kawazoe, Y.; Mita, Y. *Nature* **2005**, *436*, 238−241. (d) Millward, A. R.; Yaghi, O. M. *J. Am. Chem. Soc.* **2005**, *127*, 17998−17999. (e) Ferey, G. *Chem. Soc. Rev.* **2008**, *37*, 191−214. (f) Morris, R. E.; Wheatley, P. S. *Angew. Chem., Int. Ed.* **2008**, *47*, 4966−4981. (g) Czaja, A. U.; Trukhan, N.; Müller, U. *Chem. Soc. Rev.* **2009**, *38*, 1284−1293. (h) Chen, B.; Xiang, S.; Qian, G. *Acc. Chem. Res.* **2010**, *43*, 1115−1124. (i) Zhou, H.-C.; Long, J. R.; Yaghi, O. M. *Chem. Rev.* **2012**, *112*, 673−674. (j) Li, J.-R.; Sculley, J.; Zhou, H.-C. *Chem. Rev.* **2012**, *112*, 869−932. (k) Schneemann, A.; Henke, S.; Schwedler, I.; Fischer, R. A. *ChemPhysChem* **2014**, *15*, 823−839. (l) Evans, J. D.; Sumby, C. J.; Doonan, C. J. *Chem. Soc. Rev.* **2014**, *43*, 5933−5951.

(2) (a) Caskey, S. R.; Wong-Foy, A. G.; Matzger, A. J. *J. Am. Chem. Soc.* **2008**, *130*, 10870−10871. (b) Dincă, M.; Long, J. R. *Angew. Chem., Int. Ed.* **2008**, *47*, 6766−6779. (c) Dietzel, P. D. C.; Besikiotis, V.; Blom, R. *J. Mater. Chem.* **2009**, *19*, 7362−7370. (d) Herm, Z. R.; Swisher, J. A.; Smit, B.; Krishna, R.; Long, J. R. *J. Am. Chem. Soc.* **2011**, *133*, 5664−5667. (e) Mason, J. A.; Sumida, K.; Herm, Z. R.; Krishna, R.; Long, J. R. *Energy Environ. Sci.* **2011**, *4*, 3030−3040. (f) Bloch, E. D.; Murray, L. M.; Queen, W. L.; Chavan, S.; Maximoff, S. N.; Bigi, J. P.; Krishna, R.; Peterson, V. K.; Grandjean, F.; Long, G. J.; Smit, B.; Bordiga, S.; Brown, C. M.; Long, J. R. *J. Am. Chem. Soc.* **2011**, *133*, 14814−14822. (g) Bloch, E. D.; Queen, W. L.; Krishna, R.; Zadrozny, J. M.; Brown, C. M.; Long, J. R. *Science* **2012**, *335*, 1606−1610. (h) Geier, S. J.; Mason, J. A.; Bloch, E. D.; Queen, W. L.; Hudson, M. R.; Brown, C. M.; Long, J. R. *Chem. Sci.* **2013**, *4*, 2054−2061. (i) Sumida, K.; Rogow, D. R.; Mason, J. A.; McDonald, T. M.; Bloch, E. D.; Herm, Z. R.; Bae, T.-H.; Long, J. R. *Chem. Rev.* **2012**, *112*, 724−781. (j) Herm, Z. R.; Krishna, R.; Long, J. R. *Microporous Mesoporous Mater.* **2012**, *151*, 481−487. (k) Peng, Y.; Krungleviciute, V.; Eryazici, I.; Hupp, J. T.; Farha, O. K.; Yildirim, T. *J. Am. Chem. Soc.* **2013**, *135*, 11887−11894. (l) Mason, J. A.; Veenstra, M.; Long, J. R. *Chem. Sci.* **2014**, *5*, 32−51. (m) Herm, Z. R.; Bloch, E. D.; Long, J. R. *Chem. Mater.* **2014**, *26*, 323−338. (n) Duan, X.; He, Y.; Cui, Y.; Yang, Y.; Krishna, R.; Chen, B.; Qian, G. *RSC Adv.* **2014**, *4*, 23058−23063.

(3) Lee, K.; Isley, W. C., III; Dzubak, A. L.; Verma, P.; Stoneburner, S. J.; Lin, L.−C.; Howe, J. D.; Bloch, E. D.; Reed, D. A.; Hudson, M. R.; Brown, C. M.; Long, J. R.; Neaton, J. B.; Smit, B.; Cramer, C. J.; Truhlar, D. G.; Gagliardi, L. *J. Am. Chem. Soc.* **2014**, *136*, 698−704.

(4) (a) Colombo, V.; Galli, S.; Choi, H. J.; Han, G. D.; Maspero, A.; Palmisano, G.; Masciocchi, N.; Long, J. R. *Chem. Sci.* **2011**, *2*, 1311−1319. (b) Anderson, J. S.; Gallagher, A. T.; Mason, J. A.; Harris, T. D. *J. Am. Chem. Soc.* **2014**, *136*, 16489−16492.

(5) (a) Baschuk, J. J.; Li, X. *Int. J. Energy Res.* **2001**, *25*, 695−713. (b) Cheng, X.; Shi, Z.; Glass, N.; Zhang, L.; Zhang, J.; Song, D.; Liu, Z.-S.; Wang, H.; Shen, J. *J. Power Sources* **2007**, *165*, 739−756. (c) Hooper, C. W. *Catalytic Ammonia Synthesis: Fundamentals and Practice*; Jennings, J. R., Ed.; Springer: New York, 1991.

(6) (a) Dutta, N. N.; Patil, G. S. *Gas Sep. Purif.* **1995**, *9*, 277−283. (b) Kerry, F. G. *Industrial Gas Handbook: Gas Separation and Purification*; CRC: Boca Raton, FL, 2007.

(7) (a) McCandless, F. P. *Ind. Eng. Chem. Process Des. Dev.* **1972**, *11*, 470−478. (b) DiMartino, S. P.; Glazer, J. L.; Houston, C. D.; Schott, M. E. *Gas Sep. Purif.* **1988**, *2*, 120−125.

(8) (a) Tamon, H.; Kitamura, K.; Okazaki, M. *AIChE J.* **1996**, *42*, 422. (b) Golden, T. C.; Guro, D. E.; Kratz, W. C.; Sabram, T. E. *Fundamentals of Adsorption*; Meunier, F., Ed.; Elsevier: Amsterdam, The Netherlands, 1998. (c) Miyajima, H.; Kodama, A.; Goto, M.; Hirose, T. *Adsorption* **2005**, *11*, 625−630.

(9) (a) Kohl, A. L.; Reisenfeld, F. C. *Gas Purification*, 3rd ed.; Gulf Publishing: Houston, TX, 1979. (b) Haase, D. J.; Walker, D. G. *Chem. Eng. Prog.* **1974**, *70*, 74.

(10) (a) Munusamy, K.; Sethia, G.; Patil, D. V.; Somayajulu Rallapalli, P. B.; Somani, R. S.; Bajaj, H. C. *Chem. Eng. J.* **2012**, *195*, 359−368. (b) Chavan, S.; Vitillo, J. G.; Groppo, E.; Bonino, F.; Lamberti, C.; Dietzel, P. D. C.; Bordiga, S. *J. Phys. Chem. C* **2009**, *113*, 3292−3299. (c) Sato, H.; Kosaka, W.; Matsuda, R.; Hori, A.; Hijikata, Y.; Belosludov, R. V.; Sakaki, S.; Takata, M.; Kitagawa, S. *Science* **2014**, *343*, 167−170. (d) Bloch, E. D.; Hudson, M. R.; Mason, J. A.; Chavan, S.; Crocella, V.; Howe, J. D.; Lee, K.; Dzubak, A. L.; Queen, W. L.; Zadrozny, J. M.; Geier, S. J.; Lin, L.-C.; Gagliardi, L.; Smit, B.; Neaton, J. B.; Bordiga, S.; Brown, C. M.; Long, J. R. *J. Am. Chem. Soc.* **2014**, *136*, 10752−10761. (e) Peng, J.; Xian, S.; Xiao, J.; Huang, Y.; Xia, Q.; Wang, H.; Li, W. *Chem. Eng. J.* **2015**, *270*, 282−289.

(11) (a) Denysenko, D.; Grzywa, M.; Jelic, J.; Reuter, K.; Volkmer, D. *Angew. Chem., Int. Ed.* **2014**, *53*, 5832−5836. (b) Gonzalez, M. I.; Bloch, E. D.; Mason, J. A.; Teat, S. J.; Long, J. R. *Inorg. Chem.* **2015**, *54*, 2995−3005.

(12) (a) Halder, G. J.; Kepert, C. J.; Moubaraki, B.; Murray, K. S.; Cashion, J. D. *Science* **2002**, *298*, 1762−1765. (b) Bonhommeau, S.; Molnar, G.; Galet, A.; Zwick, A.; Real, J. A.; McGarvey, J. J.; Bousseksou, A. *Angew. Chem., Int. Ed.* **2005**, *44*, 4069−4073. (c) Quesada, M.; de la Pena-O'Shea, V. A.; Aromi, G.; Geremia, S.; Massera, C.; Roubeau, O.; Gamez, P.; Reedijk, J. *Adv. Mater.* **2007**, *19*, 1397−1402. (d) Neville, S. M.; Moubaraki, B.; Murray, K. S.; Kepert, C. J. *Angew. Chem., Int. Ed.* **2007**, *46*, 2059−2062. (e) Neville, S. M.; Halder, G. J.; Chapman, K. W.; Duriska, M. B.; Southon, P. D.; Cashion, J. D.; Letard, J. F.; Moubaraki, B.; Murray, K. S.; Kepert, C. J. *J. Am. Chem. Soc.* **2008**, *130*, 2869−2876. (f) Halder, G. J.; Chapman, K. W.; Neville, S. M.; Moubaraki, B.; Murray, K. S.; Letard, J.-F.; Kepert, C. J. *J. Am. Chem. Soc.* **2008**, *130*, 17552−17652. (g) Ohba, M.; Yoneda, K.; Agusti, G.; Munoz, M. C.; Gaspar, A. B.; Real, J. A.;

DOI: 10.1021/jacs.6b00248
J. Am. Chem. Soc. 2016, 138, 5594−5602

Yamasaki, M.; Ando, H.; Nakao, Y.; Sakaki, S.; Kitagawa, S. *Angew. Chem., Int. Ed.* **2009**, *48*, 4767−4771. (h) Southon, P. D.; Liu, L.; Fellows, E. A.; Price, D. J.; Halder, G. J.; Chapman, K. W.; Moubaraki, B.; Murray, K. S.; Letard, J. F.; Kepert, C. J. *J. Am. Chem. Soc.* **2009**, *131*, 10998−11009. (i) Ohtani, R.; Yoneda, K.; Furukawa, S.; Horike, N.; Kitagawa, S.; Gaspar, A. B.; Munoz, M. C.; Real, J. A.; Ohba, M. *J. Am. Chem. Soc.* **2011**, *133*, 8600−8605. (j) Salles, F.; Maurin, G.; Serre, C.; Llewellyn, P. L.; Knofel, C.; Choi, H. J.; Filinchuk, Y.; Oliviero, L.; Vimont, A.; Long, J. R.; Ferey, G. *J. Am. Chem. Soc.* **2010**, *132*, 13782−13788.

(13) (a) Garcia, Y.; Niel, V.; Munoz, M. C.; Real, J. A. *Top. Curr. Chem.* **2004**, *233*, 229−257. (b) Van Koningsbruggen, P. J. *Top. Curr. Chem.* **2004**, *233*, 123−149. (c) Kitchen, J. A.; Brooker, S. *Coord. Chem. Rev.* **2008**, *252*, 2072−2092. (d) Kitchen, J. A.; White, N. G.; Jameson, G. N. L.; Tallon, J. L.; Brooker, S. *Inorg. Chem.* **2011**, *50*, 4586−5497. (e) Krober, J.; Audiere, J. P.; Claude, R.; Codjovi, E.; Kahn, O.; Haasnoot, J. G.; Groliere, F.; Jay, C.; Bousseksou, A.; Linares, J.; Varret, F.; Gonthier-Vassal, A. *Chem. Mater.* **1994**, *6*, 1404−1412. (f) Schneider, C. J.; Cashion, J. D.; Chilton, N. F.; Etrillard, C.; Fuentealba, M.; Howard, J. A. K.; Letard, J.-F.; Milsmann, C.; Moubaraki, B.; Sparkes, H. A.; Batten, S. R.; Murray, K. S. *Eur. J. Inorg. Chem.* **2013**, *2013*, 850−864.

(14) Demessence, A.; D'Alessandro, D. M.; Foo, M. L.; Long, J. R. *J. Am. Chem. Soc.* **2009**, *131*, 8784−8786.

(15) (a) Dincă, M.; Dailly, A.; Liu, Y.; Brown, C. M.; Neumann, D. A.; Long, J. R. *J. Am. Chem. Soc.* **2006**, *128*, 16876−16883. (b) Dincă, M.; Han, W. S.; Liu, Y.; Dailly, A.; Brown, C. M.; Long, J. R. *Angew. Chem., Int. Ed.* **2007**, *46*, 1419−1422. (c) Sumida, K.; Horike, S.; Kaye, S. S.; Herm, Z. R.; Queen, W. L.; Brown, C. M.; Grandjean, F.; Long, G. J.; Dailly, A.; Long, J. R. *Chem. Sci.* **2010**, *1*, 184−191. (d) Biswas, S.; Maes, M.; Dhakshinamoorthy, A.; Feyand, M.; De Vos, D. E.; Garcia, H.; Stock, N. *J. Mater. Chem.* **2012**, *22*, 10200−10209. (e) Liao, J. H.; Chen, W. T.; Tsai, C. S.; Wang, C. C. *CrystEngComm* **2013**, *15*, 3377−3384.

(16) (a) Bordiga, S.; Regli, L.; Bonino, F.; Groppo, E.; Lamberti, C.; Xiao, B.; Wheatley, P. S.; Morris, R. E.; Zecchina, A. *Phys. Chem. Chem. Phys.* **2007**, *9*, 2676−2685. (b) Yoon, J. W.; Seo, Y.-K.; Hwang, Y. K.; Chang, J.-S.; Leclerc, H.; Wuttke, S.; Bazin, P.; Vimont, A.; Daturi, M.; Bloch, E.; Llewellyn, P. L.; Serre, C.; Horcajada, P.; Greneche, J.-M.; Rodrigues, A. E.; Ferey, G. *Angew. Chem., Int. Ed.* **2010**, *49*, 5949−5952.

(17) (a) Yoshida, Z.; Sugimoto, H.; Ogoshi, H. *Adv. Chem. Ser.* **1980**, *191*, 307. (b) Strauss, S. H.; Holm, R. H. *Inorg. Chem.* **1982**, *21*, 863−868. (c) Klose, A.; Hesschenbrouck, J.; Solari, E.; Latronico, M.; Floriani, C.; Re, N.; Chiesi-Villa, A.; Rizzoli, C. *J. Organomet. Chem.* **1999**, *591*, 45. (d) Benito-Garagorri, D.; Lagoja, I.; Veiros, L. F.; Kirchner, K. A. *Dalton Trans.* **2011**, *40*, 4778−4792.

(18) Gütlich, P.; Bill, E.; Trautwein, A. X. *Mossbauer Spectroscopy and Transition Metal Chemistry*; Springer-Verlag: Berlin, 2007.

(19) Neese, F.; Pantazis, D. A. *Faraday Discuss.* **2011**, *148*, 229−238.

(20) (a) Cantalupo, S. A.; Fiedler, S. R.; Shores, M. P.; Rheingold, A. L.; Doerrer, L. H. *Angew. Chem., Int. Ed.* **2012**, *51*, 1000−1005. (b) Pascualini, M. E.; Di Russo, N. V.; Thuijs, A. E.; Ozarowski, A.; Stoian, S. A.; Abboud, K. A.; Christou, G.; Veige, A. S. *Chem. Sci.* **2015**, *6*, 608−612.

(21) Sachse, A.; Demeshko, S.; Meyer, F. *Dalton Trans.* **2009**, 7756−7764.

(22) (a) Peng, S.-M.; Ibers, J. A. *J. Am. Chem. Soc.* **1976**, *98*, 8032−8036. (b) Goedken, V. L.; Peng, S.-M.; Molin-Norris, J.; Park, Y. *J. Am. Chem. Soc.* **1976**, *98*, 8391−8400.

DOI: 10.1021/jacs.6b00248
J. Am. Chem. Soc. 2016, 138, 5594−5602